Adaptive Matching Transmitter With Dual-Band Antenna for Intraoral Tongue Drive System

Fanpeng Kong ⓘ, *Student Member, IEEE*, Muhammad Zada ⓘ, Hyoungsuk Yoo ⓘ, *Member, IEEE*, and Maysam Ghovanloo ⓘ, *Senior Member, IEEE*

Abstract—The intraoral Tongue Drive System (iTDS) is a wireless assistive technology that detects users' voluntary tongue gestures, and converts them to user-defined commands, enabling them to access computers and navigate powered wheelchairs. In this paper, we presented a transmitter (Tx) with adaptive matching and three bands (27, 433, and 915 MHz) to create a robust wireless link between iTDS and an external receiver (Rx) by addressing the effects of external RF interference and impedance variations of the Tx antenna in the dynamic mouth environment. The upper two Tx bands share a dual-band antenna, while the lower band drives a coil. The Tx antenna is simulated in a simplified human mouth model in HFSS as well as a real human head model. The adaptive triple-band Tx chip was fabricated in a 0.35-μm 4P2M standard CMOS process. The Tx chip and antenna have been characterized in a human subject as part of an iTDS prototype under open- and closed-mouth scenarios, which present the peak gain of -24.4 and -15.63 dBi at 433 and 915 MHz, respectively. Two adaptive matching networks for these bands compensate variations of the Tx antenna impedance via a feedback mechanism. The measured S_{11} tuning range of the proposed network can cover up to 60 and 75 jΩ at 433 and 915 MHz, respectively.

Index Terms—Assistive technologies, adaptive matching, dual-band antenna, intraoral Tongue Drive System.

I. INTRODUCTION

A CONSIDERABLE number of people are living with paralysis, resulted from various causes from spinal cord injury (SCI) to certain neurological diseases [1]. Severe physical disability leads to major difficulties in daily living due to lack of function, and results in loss of independence. Even though the caregivers, friends and family can provide some level of assistance for individuals with disabilities, the cost of care is quite substantial and affordable only to a limited number of people, and constrained to limited hours or days for others. Therefore, to improve the level of independence for these individuals and improve their quality of life, assistive technologies (AT) are developed to employ some of their remaining abilities, such as head and eye movements, voice, and brain signals [2]–[7]. The existing ATs, however, have limitations, such as robustness, intuitiveness, and compatibility. For example, the EEG-based brain-computer interfaces (BCI) are susceptible to motion artifacts [8], [9], and the voice recognition systems are only suitable in the quiet environments [10]. There is a need for a new AT that is noninvasive, unobtrusive, and robust enough for operation in various environments. It also needs to be simple, and offers a broad coverage of various end users.

The Tongue Drive System (TDS) is a wireless and wearable tongue-operated AT that can provide certain control functions over a wide range of applications, taking advantages of inherent abilities of the human tongue [11]. Most individuals with SCI and other neurological diseases can still easily move their tongues voluntarily without training or concentration because of the direct connection between the tongue and brain through cranial nerves. TDS operates by monitoring the changes in magnetic field, generated by a small permanent magnetic tracer, the size of a lentil, which is attached near the tip of the tongue, when the tongue moves, using four 3-axial magnetic sensors inside the mouth or near the cheeks [12]. A universal interface wirelessly receives the magnetic field information as the raw data, and deliver it to a PC or smartphone to be analyzed by a sensor signal processing (SSP) algorithm, which uses pattern recognition to detect the intended tongue commands.

The TDS has been designed in two forms: First, in the form of a wireless headset, to be referred to as the external TDS (eTDS), which functionality has already been clinically tested [13]. A new multimodal version of the eTDS (mTDS) has also been developed, which combines head tracking and speech recognition with the tongue movements to give the end users even more options to control their environments [14]. Second, in the form of an intraoral Tongue Drive System (iTDS), like a dental retainer, which was developed to give the users more privacy with no apparent body-worn component, and the magnetic sensors more mechanical stability by fixating the sensor positions with respect to the upper or lower jaw [15].

The latest version of iTDS is designed as an arch-shaped dental retainer that clasps onto the teeth, with the electronics and a rechargeable battery being located in the mouth buccal shelf area, as shown in Fig. 1, which also shows the other key components of the iTDS. The raw magnetic field data from four 3-axial magnetic sensors (LSM303D, STMicroelectronics)
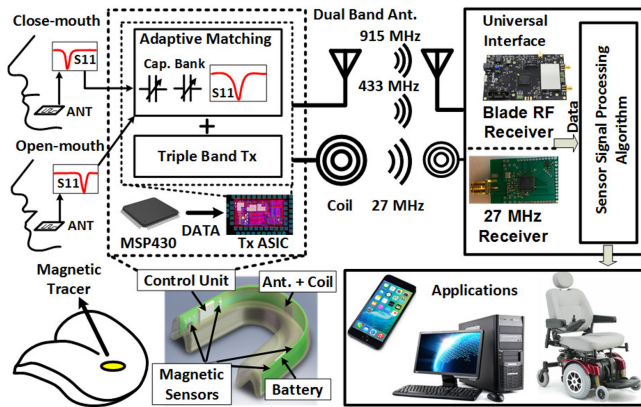
Fig. 1. Conceptual view of the intraoral Tongue Drive System (iTDS) with its key components and potential target applications.

is delivered to an ultra-low power MSP430 microcontroller (MCU) (Texas Instruments, Dallas, TX) through its serial peripheral interface (SPI) bus and packetized, before being fed into a 3-band custom-designed application specific integrated circuit (ASIC) transmitter (Tx). The 3-band Tx chip, which is the focus of this article, is designed to wirelessly transmit the packets either at 433 MHz or 915 MHz by sharing a small dual-band antenna. The third band at 27 MHz utilizes a coil for data transmission in the near-field, which is also used to wirelessly charge the battery at 13.56 MHz. The external receiver (Rx) can be a commercially-available software define radio (SDR), such as bladeRF (Nuand LLC, Rochester, NY) [16], which also has a built-in field-programmable gate array (FPGA) that can be used to implement the SSP algorithm.

A key objective in design of the iTDS is maintaining a robust wireless communication with the external Rx, particularly for safety-critical tasks such as wheelchair navigation, while keeping the power consumption low to extend the small battery operating time beyond one day. The main challenges are the considerable power loss in the tissue, which is affected by the choice of carrier frequency, the compromise between the user comfort and the size of battery, antenna, and iTDS electronics, and dealing with the dynamic environment of the mouth, which results in detuning the Tx antenna because of the movements of the jaw and the tongue. Moreover, there are always external sources of noise and interface that can disrupt the wireless link by lowering the signal-to-noise ratio (SNR) on the Rx side. As a measure of safety and robustness, it is more suitable to have multiple bands instead of only one band. Because if operation of one band is severely affected by the external interference, another band would be available to switch to, and continue the system operation.

Previously, we developed a version of the iTDS using only commercial-off-the-shelf (COTS) components, plus a custom high-gain intraoral antenna for 2.4 GHz carrier frequency to achieve a robust wireless communication [17]. However, 2.4 GHz is a crowded band and suffers from considerable loss in the tissue, which result in a low specific absorption rate (SAR) limit [18], [19]. In our previous work, we identified better choices within the Industrial-Scientific-Medical (ISM) band,

and presented a dual band system which operated at 27 MHz and 433 MHz [15], [20]. This system had only one far-field operating frequency, at 433 MHz, which in the absence of an external 27 MHz receiver coil, is still prone to interference. In this paper, we present a Tx ASIC with a secondary far-field operating frequency in 915 MHz, which is away from the busy 2.4 GHz band, and offers an alternative, even in the absence of a near-field external Rx coil.

To address the dynamic intraoral environment, an adaptive matching mechanism is implemented on the ASIC to compensate for the changes in the antenna impedance due to jaw and tongue movements. Adding dynamic matching components, such as capacitors, ahead of the antenna is common [21]–[25]. However, these discrete components occupy a large space, and provide a limited number of matching combinations. For instance, four discrete capacitors used in the matching network of [21] offer only 16 matching options, which might be too coarse for this application. Even though fully-integrated matching networks are reported in the literature [26], [27], these implementations are rather too complex and occupy large chip area for the iTDS application.

In this work, we present a triple-band Tx ASIC with hybrid adaptive matching, assisted by a COTS ultra-low power MCU to achieve sufficient resolution, while reducing the on-chip footprint by avoiding complexity. We are also presenting a dual-band Tx antenna, operating at 433 MHz and 915 MHz, which dimensions are specifically suitable for intraoral applications. Section II describes the Tx ASIC design and its key building blocks. The adaptive matching mechanism is presented in Section II-B. The dual-band antenna design is described in Section III, including simulation results, followed by ASIC measurements and antenna characterization results in Section IV, and conclusion in Section V.

II. SYSTEM ARCHITECTURE

Block diagram of the triple-band Tx ASIC with its off-chip components is shown in Fig. 2. Two low dropout (LDO) linear regulators convert the rechargeable Li-Po battery voltage to 1.8 V, one for analog blocks and the other for digital blocks, and a band-gap reference (BGR) generates the required bias currents. Twelve magnetic sensors (3-axes × 4 LSM303) are sampled at 100 Hz each, with each sample being 2-bytes, and packetized in the MCU to generate raw data packets that are 30 bytes long. The ASIC includes a digital control block for buffering the data packets and generating control signals to select different bands. Data packets are serially loaded onto an on-chip shift register at a rate of 24 kb/s, while an additional 2 command lines between the MCU and the ASIC activate the desired Tx band. In this early prototype, switching from one band to another will be done by the iTDS users, who can switch the active band by placing their tongues at a specific position, e.g., holding the tongue against the right cheek for >3 s. This will trigger a special tongue command that is detected locally in the MCU by simply elevating the absolute value of a designated magnetic sensor output above a certain threshold for a designated period. When the original connection is lost, the external
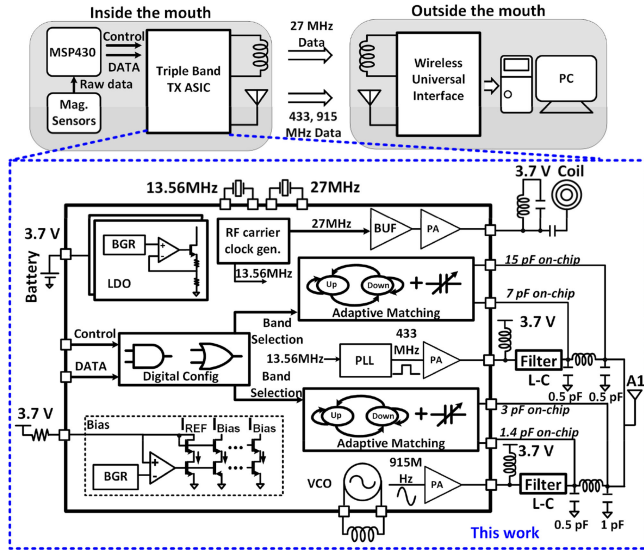
Fig. 2. Block diagram of the iTDS triple-band transmitter ASIC with its off-chip components.

Fig. 3. Schematic diagram of the transmitters at (a) 27 MHz, (b) 915 MHz, and (c) 433 MHz.

SDR-Rx keeps searching for the handshaking packet from the iTDS in different bands at initialization. Once the handshaking signal is captured at a specific band, the communication between the iTDS and SDR-Rx will be established in that band. If the connection is lost again, the SDR-Rx goes back to the searching state till another handshaking packet is detected.

A. Transmitters

Three transmitters operating at 27 MHz, 433 MHz, and 915 MHz, respectively, are included on-chip, all of which utilize on-off-keying (OOK) modulation scheme. In 27 MHz band, signal is transmitted through a coil for near field communication. The other two transmitters share the same dual-band antenna that is discussed in Section III. The default band for the iTDS is 27 MHz because it shows the lowest attenuation in human body, and consumes minimum power for near-field communication [21]. However, some citizen radios and short-distance applications, such as remote-controlled toys and Walkie-Talkies, also use this band, presenting possible sources of external interference for the iTDS [18]. The 433 MHz band was selected because of its proximity to the Medical Implant Communication Service (MICS) band, which is within 402–405 MHz, and utilized in some implantable medical devices (IMD) [29], [30], and yet it does not interfere with this band. Finally, 915 MHz was also adopted in occasions when the other two bands are occupied because it is less crowded than 2.4 GHz, while more power transmission is permitted [31].

The three-band Tx schematics are shown in Fig. 3. The 27 MHz Tx consists of a power amplifier (PA) and a buffer to realize the OOK by turning it on and off [21]. A higher power option is implemented by adding an additional current source in parallel. The 433 MHz Tx is shown in Fig. 3(c), including a phase locked loop (PLL) [32], followed by a PA [21]. A frequency divider divides the carrier signal, which is generated by the voltage controlled ring oscillator (VCRO) in the
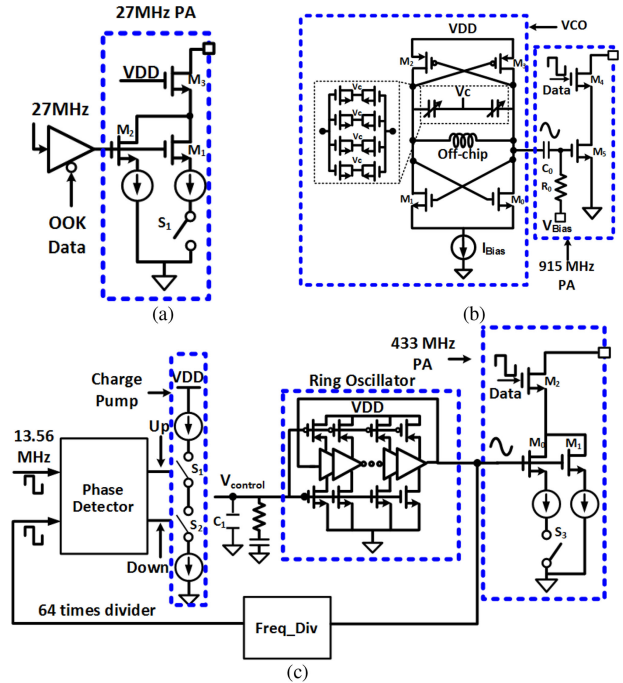
PLL, by a factor of 64 before it is compared with a crystal-based 13.56 MHz reference clock. A control voltage, $V_{control}$, varies the pull up and pull down currents of each inverter in the VCRO to adjust its delay, and consequently the carrier frequency. The phase difference between the carrier signal and the reference clock is produced by a phase detector, controlling a charge pump. $V_{control}$ is generated by charging and discharging a capacitor, C_1, at the output of the charge pump. An off-chip resistor in series with a capacitor is added at the output of the charge pump to maintain stability of the PLL. These components form a feedback loop that keeps the output and input signals in phase, locking the carrier frequency at 433 MHz. The 433 MHz PA has the same topology as 27 MHz.

The main component of the 915 MHz Tx is a voltage control LC-oscillator (VCO) with an off-chip inductor, followed by a PA [33]. Compared to 433 MHz band, which is more likely to be interfered by other medical or implantable devices around the end users, 915 MHz band is less noisy, allowing for a larger frequency tolerance. Therefore, at 915 MHz, a VCO has been adopted instead of adding PLL, which increases power consumption as well as chip and PCB areas by requiring another reference frequency generator. Four pairs of NMOS transistors are connected across the VCO output as varactors. The capacitances of the varactors are controlled by an external voltage, which is used to oppose the carrier frequency drifts. OOK is realized by turning on and off the cascode transistor, M_4, on top of the PA.

B. Adaptive Matching

The dynamic intraoral environment detunes the antenna, increasing the reflected power and reducing the desired power
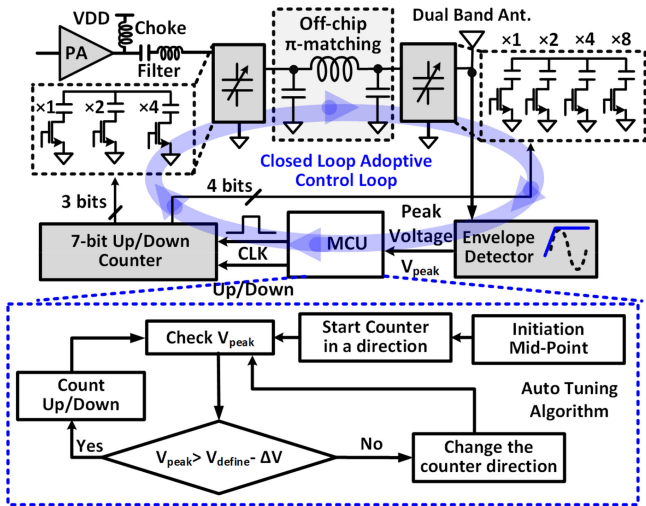
Fig. 4. Schematic diagram of the adaptive matching network, including the capacitor banks, feedback control loop, and matching algorithm flowchart.

Fig. 5. (a) Schematic diagram of the peak detector block. (b) Simulated transfer function of the peak detector at 433 MHz and 915 MHz.

transmitted from the iTDS. Unlike many other transmission scenarios, in which Tx operates in a stable environment, or its output power is increased to satisfy minimum SNR at the Rx input in the worst case condition, it is necessary to implement an adaptive matching mechanism between the Tx and antenna to compensate for the effects of detuning.

In the proposed Tx design, we have added two adaptive matching networks for 433 MHz and 915 MHz, but not for the 27 MHz because the human body, with all the dynamic changes in the intraoral environments, is transparent to magnetic field at this frequency, and has a small effect on near-field inductive coupling [34]. The 433 MHz and 915 MHz transmitters have similar output matching topologies, shown in Figs. 2 and 4, consisting of a choke inductor, a series LC-filter, and a variable π-matching network, which in turn includes two capacitor banks, an up-down counter, and an peak detector. The capacitor banks provide 1 pF and 0.2 pF matching resolution for 433 MHz and 915 MHz, respectively. Three-bit and four-bit binary-weighted on-chip poly-insulator-poly (PIP) capacitor banks are connected at the input and output nodes of the off-chip π-matching LC-tank, providing a total of 7 pF and 1.4 pF capacitance selection ranges for 433 MHz and 915 MHz at the input nodes, and 15 pF and 3 pF variable capacitance at the output nodes for 433 MHz and 915 MHz, respectively.

Each capacitor bank in the π-network is controlled by a 7-bit up-down counter, which can keep the antenna matched even though it might be detuned, thus improving the output power level. The mismatch detection and correction is based on the amplitude of the output signal fed to the antenna, which is picked up by a peak detector, and digitized by the MCU. Since the cascode structure has been used in both 433 MHz and 915 MHz PAs, the load impedance variations do not change the input impedance of the PAs much, keeping the voltage swing at the input of the PA constant at the same amount of input power [35]. Therefore, the voltage at the PA output is primarily dependent on its load impedance, which include the matching network and antenna.
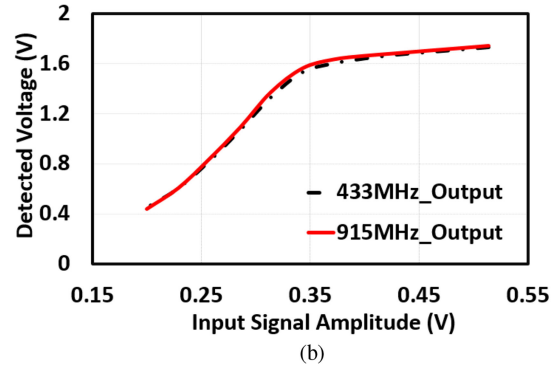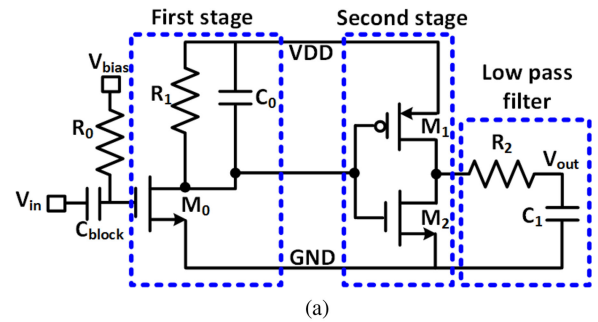
The peak detector block is shown in Fig. 5(a), which consists of an envelope detector circuit, which uses a blocking capacitor, C_{block}, in series with the gate of M_0, as an envelope detector together with an RC-network in the drain, a common-source envelope amplifier as the second stage, followed by a low pass filter to reduce ripples in the output voltage, V_{peak} [36]. When the input signal increases, the output of the M_0 decreases from VDD, and the PMOS transistor M_1 begins to charge C_1. On the other hand, once input signal decreases, M_2 starts to discharge C_1 to a specific level. In this application, the peak detector should provide large input impedance to avoid degradation of the PA performance, and fast detection time [35]. The simulated input impedance of the peak detector was 13.67 kΩ and 11.74 kΩ for 433 MHz and 915 MHz, respectively. Fig. 5(b) shows the simulated output voltage of the detector, showing its linear range, based on the input amplitude [35].

Since every matching adjustment takes multiple steps, such as V_{peak} detection, comparison, and counter sweep, it is necessary to minimize the detection time of the peak detector. However, there is a trade-off between the detection time and the output voltage ripple. A large C_1 reduces the output ripple, but increases the detector response time by taking longer to charge and discharge. Another possible solution is to increase the sizes of M_1 and M_2. In [35], it is suggested that 2 mV output voltage ripple and 0.5 μs detection time are suitable, which are the values adopted for this design in order to strike a balance between the voltage ripple and detection time. The simulation shows the actual detection time is 0.45 μs.

The adaptive matching mechanism is depicted in Fig. 4, which is implemented in the MCU. A short initialization period is required for the adaptive tuning, in which the up/down counter

starts from the mid-point, while the MCU continuously samples V_{peak} across the antenna via the peak detector block. The 7-bit counter counts in a certain direction until V_{peak} at the antenna reach within the vicinity of V_{define}, which is the voltage correlated with the transmitted power in matched condition [37]. The MCU changes counter direction when V_{peak} drops by ΔV, which is 20 mV in this case, below V_{define}. This simple tracking mechanism ensures the Tx antenna is always tuned near the original transmitted power level (not necessarily the optimal matching condition), despite dynamic changes in the oral environment, thus reducing the power loss and improving the wireless link robustness. An array of NMOS transistors are used to switch the capacitor banks. According to [35], if the Q-factor of switched capacitors is lower than 20, the power loss on these capacitors will be substantial. Therefore, we sized the switches to have Q-factor of binary scaled capacitor in the on-state to be >30 to minimize the power loss. The capacitor values of each bank were selected based on the method in [22].

Based on post layout simulation results, the actual detection time for the envelope detector is 0.45 μs. We have long rising and falling times since large NMOS transistors are adopted as switches for the capacitor banks. From simulations, 1.82 μs is needed for a capacitor to switch on and off completely. Comparison is done in the MSP430 MCU, which has 120 ns as the response time for its internal comparator [38]. Therefore, it is required 2.39 μs to check one capacitor combination. We can assume 3 μs to check one matching combination. Therefore, a total of 0.38 ms is required to check all possible 128 combinations.

III. DUAL BAND ANTENNA DESIGN

Considering the limited intraoral space, a small dual-band antenna at 433 MHz and 915 MHz was designed to achieve reliable communication between iTDS and SDR-Rx. To fit the arch-shaped iTDS, the planar antenna was designed within a rectangular space on flexible substrate to be placed in front of the incisors.

A. Antenna Design

The structure and dimensions of the proposed antenna are depicted in Fig. 6(a)–6(c), presenting the front view, radiating patch, and top view of the antenna, respectively. The dielectric material, Roger RT/duriod 6010 ($\varepsilon_r = 10.2$, tan $\delta = 0.0035$, thickness = 0.63 mm), is chosen as the substrate because of its flexibility and high relative permittivity. To hermetically seal the antenna, it is coated with a 1 mm-thick silicone (Polydimethylsiloxane or PDMS) layer, which has relative permittivity of 2.68 and tangent loss of 0.04. The dimension of the antenna is optimized based on the human oral anatomy, which have been investigated in [17], occupying 266.7 mm^3 ($42 \times 10 \times 0.635$ mm^3) space within the iTDS. The radiating patch consists of two symmetrical spiral arms, which extend the antenna current path, and are connected through a 0.3 mm-thick strip, miniaturizing the size of the antenna. The width of the meandered strips plays an important role in the impedance matching. By carefully varying the width, the antenna is matched at desired
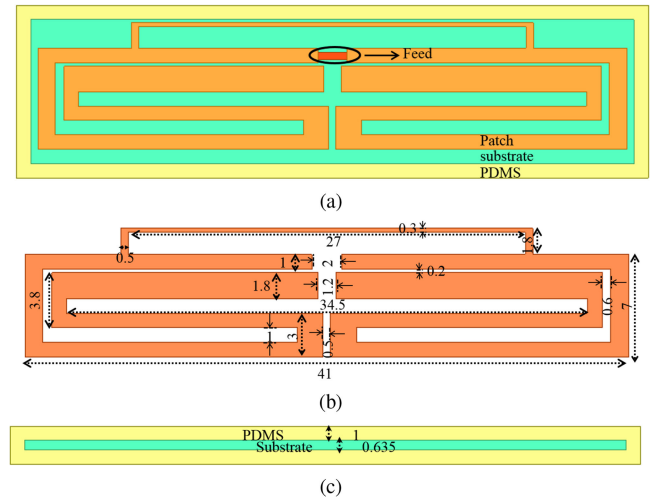

Fig. 6. Geometry of the proposed dual band antenna (unit: mm): (a) top view, (b) radiating patch, and (c) Side view.
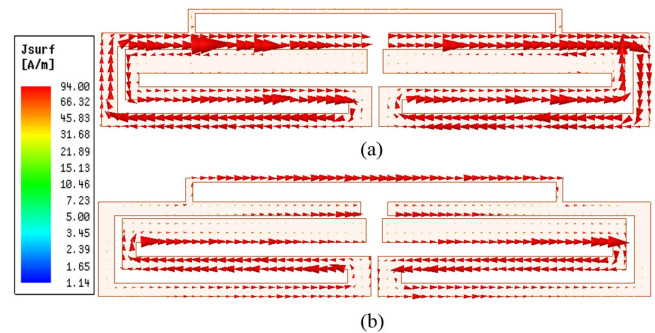

Fig. 7. Surface current distribution on the proposed dual band antenna at: (a) 433 MHz. (b) 915 MHz.

ISM bands. A 50 Ω coaxial feed, shown in Fig. 6(a), merges the ends of the two arms. The current distribution in the proposed dual-band antenna in 433 MHz band, shown in Fig. 7(a), shows that the entire path contributes to the radiation, while in the 915 MHz band, shown in Fig. 7(b), only the middle portion of the radiating patch contributes.

B. Simulation Setup

The dual-band antenna is designed and simulated in Ansoft HFSS in a 200×200 mm^2 multi-layer heterogeneous custom mouth model, shown in Fig. 8(a), which includes different types of tissues materials, including muscle, skin, teeth, tongue, and saliva. Properties of these tissues are depicted in Table I, and considered frequency-dependent in simulations, as described in [39]. Additionally, to validate the simulation results in our custom HFSS model, the proposed antenna was simulated in a realistic human head model in XFdtd Remcom, shown in Fig. 8(b). We also simulated the open-and closed-mouth conditions in both models. Since it is not possible to open the mouth in the realistic phantom, an air box ($63 \times 50 \times 15$ mm^3) was inserted below the upper jaw of the phantom in the open-mouth model. The return loss (S_{11}) simulation results for the proposed antenna in the HFSS and closed/open-mouth conditions in the
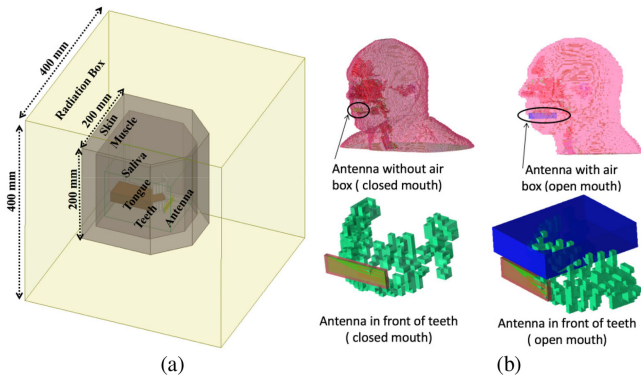
Fig. 8.   Simulation setup for the proposed antenna: (a) human mouth model in HFSS, (b) human head phantom in Remcom for open-and closed-mouth conditions.

TABLE I
DIELECTRIC PROPERTIES OF THE TISSUES

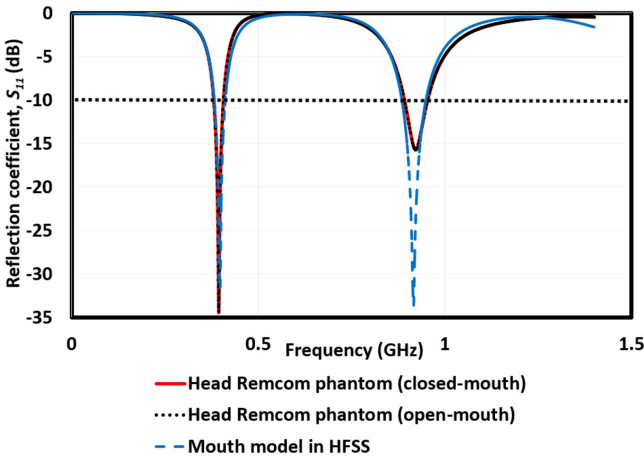| Tissue Type	433 MHz		915 MHz	
	ε_r	$\sigma[S/m]$	ε_r	$\sigma[S/m]$
Skin	46.08	0.702	41.33	0.872
Muscle	56.87	0.805	54.99	0.948
Tongue	57.38	0.783	55.23	0.942
Teeth	13.074	0.094	12.44	0.145
Saliva	77.3	0.738	76.00	0.818

Fig. 9.   Simulated reflection coefficient of the proposed dual-band antenna in HFSS and Remcom models in the open-and closed-mouth conditions.

XFdtd Remcom are shown in Fig. 9, which indicates the antenna has sufficiently low power reflection in both 433 MHz and 915 MHz bands. The -10 dB bandwidths at 433 MHz and 915 MHz are 28 MHz and 99 MHz in the HFSS mouth model, respectively. In the Remcom human head model, the bandwidth at 433 MHz is 26 MHz for open-mouth and 28 MHz for closed-mouth. At 915 MHz, the bandwidth is 61 MHz and 65 MHz for open-and closed-mouth, respectively.

Fig. 10 presents the realized gain radiation pattern of the proposed antenna in mouth model in Ansoft HFSS and Remcom
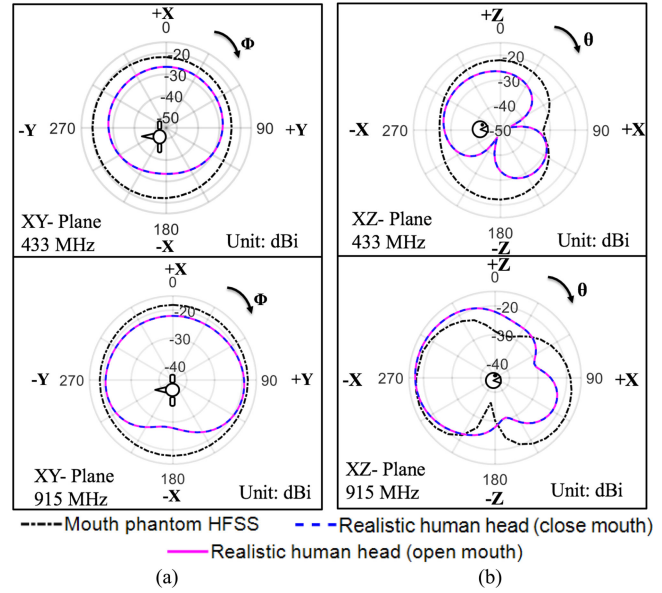

Fig. 10.   Simulated realized gain radiation pattern of the proposed antenna in HFSS and Remcom human head model at 433 MHz and 915 MHz in: (a) Azimuthal (XY plane) and (b) Elevation (XZ plane).

at 433 MHz and 915 MHz, including azimuthal (XY plane) and elevation (XZ plane). Because of the power loss in the tissue, the realized gain is below zero in every direction. When the mouth is closed, the peak realized gain at 433 MHz and 915 MHz are -19.59 dBi and -16.99 dBi in the mouth model in HFSS, respectively. Using the realistic human head model, the peak realized gain in the open-mouth case at 433 MHz and 915 MHz are -25.66 dBi and -15.08 dBi; and for the closed mouth case -26.41 dBi and -17.03 dBi, respectively. According to the simulation in the XFdtd Remcom human head model, the open-and closed-mouth show little differences and present similar radiation patterns at the desired frequency bands.

IV.   MEASUREMENT RESULTS

A.   Dual-Band Antenna

The dual-band antenna was fabricated using a milling machine and coated with PDMS after being degassed in a vacuum chamber. A U.FL to SMA cable is used to feed the antenna and connect it to a vector network analyzer (VNA) for measurement. The fabricated antenna with PDMS coating, shown in Fig. 11, was placed inside in human mouth to perform the reflection coefficient (S_{11}) measurements under open-and closed-mouth scenarios. The simulation and measurement results using XFdtd Remcom for open-and closed-mouth scenarios are compared in Fig. 12. At low frequencies, the measurement results show a slight shift from the simulation results, $\sim$30 MHz towards the higher frequencies. At high frequencies there is a very good agreement between simulation and measurement results. Measured results show the -10 dB bandwidth in open-mouth to be 25 MHz and 92 MHz at the 433 MHz and 915 MHz, respectively. When the mouth is closed, the bandwidth is 40 MHz and 65 MHz at 433 MHz and 915 MHz, respectively. These
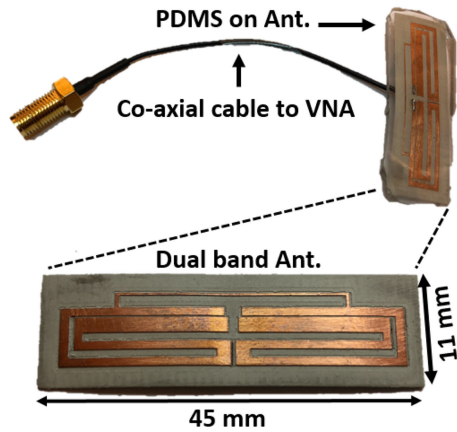
Fig. 11. Fabricated dual-band antenna on Roger substrate with PDMS coating and co-axial cable.
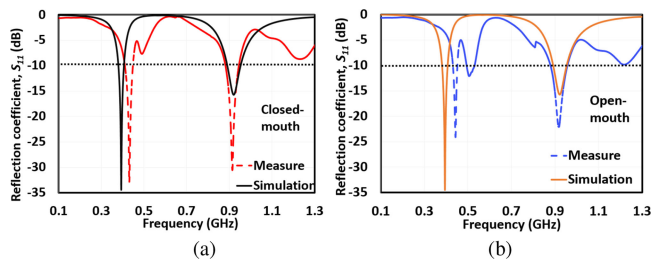

Fig. 14. The die photo of the multi-frequency transmitter system which has 1.97 mm length and 1.18 mm width.

Fig. 12. Combining measured and simulated reflection coefficient of the proposed dual band antenna in (a) closed- and (b) open-mouth conditions.

Fig. 15. Multi-frequency Tx measurement results of the output spectrums of (a) 433 MHz Tx, (b) 915 MHz Tx, and (c) 27 MHz Tx. (d) Serial data bit stream and 27 MHz OOK carrier signal at the output of the 27 MHz Tx.
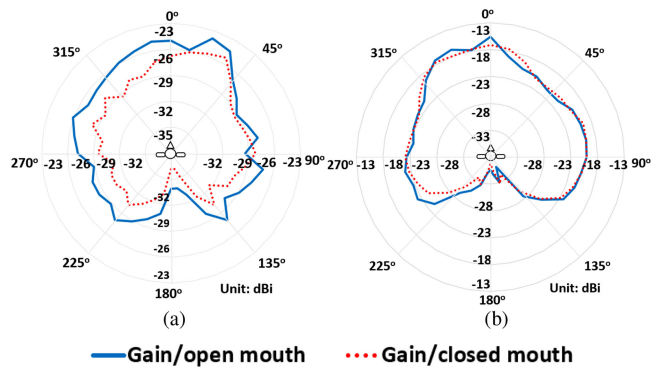

Fig. 13. Measured realized gain radiation pattern of the dual-band antenna at (a) 433 MHz and (b) 915 MHz under open-and closed-mouth conditions.

of -15.63 dBi and -17.13 dBi for the open-and closed-mouth conditions, respectively.

B. Tx Measurement Results

The adaptive multi-frequency Tx ASIC was fabricated in the TSMC 0.35-μm standard CMOS process, occupying 1.97×1.18 mm^2 of silicone real estate, as shown in Fig. 14. To validate the basic Tx functionality, we measured the output power spectrum of each individual Tx with 50-Ω spectrum analyzer input port loading, as shown in Fig. 15. Fig. 15(d) shows the transient OOK signal at 27 MHz. The output power of the Tx at 27 MHz, 433 MHz, and 915 MHz are -20.16 dBm, -23.18 dBm, and -18.77 dBm, respectively, which are lower than simulation results in [40]. Additional parasitic components on the printed circuit board (PCB), deviation from 50-Ω loading, and mismatch with the measurement cable are possible reasons for this discrepancy.

bandwidths can sufficiently cover both lower and higher ISM bands for data transmission.

To characterize the radiation pattern of the antenna, we adopted method similar to [17]. The subject stood on a rotating plate with designated rotation angles on a calibrated rooftop antenna range with the dual-band antenna in the mouth. The Rx antenna, connected to a VNA, was placed in front, 75 cm from the subject. Measurements were conducted under open-and closed-mouth conditions, with the results shown in Fig. 13. At 433 MHz, the peak gains of the proposed antenna are -24.4 dBi and -25.27 dBi for open-and closed-mouth, respectively. For 915 MHz, when the mouth was open, the antenna has peak gain
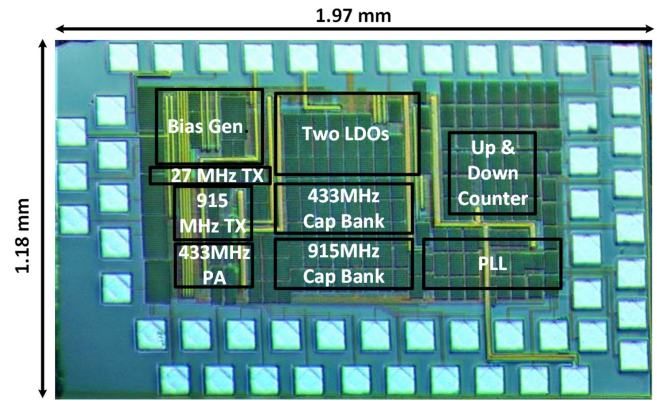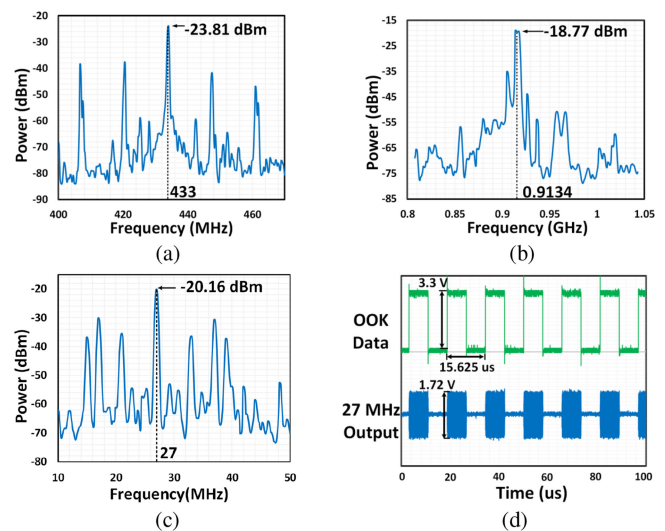
TABLE II
BENCHMARKING THE MATCHING PERFORMANCE

	TBioCAS 2012[15]	TMTT 2014[21]	JSSC 2008[41]	RFIC 2013[42]	TBioCAS 2017[27]	JSSC 2014[35]	This work
Process	0.5-μm std. CMOS	Discrete	RF-MEMS	2-μm HBT	40-nm CMOS	0.18-μm std. CMOS	0.35-μm std. CMOS
Frequency (MHz)	27/433	27, 433, 2480	900	1950	2400	2400	27/433/915
Dynamic matching	No	Yes	Yes	Yes	Yes	Yes	Yes
Matching integration	-	Off-chip	On-chip	Off-chip	On-chip	On-chip	On-chip
Detection target	-	Power	Phase	Polar	Polar	Magnitude	Magnitude
Tuner settings	-	16	32	8	32	128	128
Tuning range	-	-	75j	VSWR of 2.5	VSWR of 3	VSWR of 1.9	60jΩ@433MHz 75jΩ@915MHz
Application	iTDS	iTDS	Mobile	Mobile	Wearable/ Implantable	Mobile	iTDS
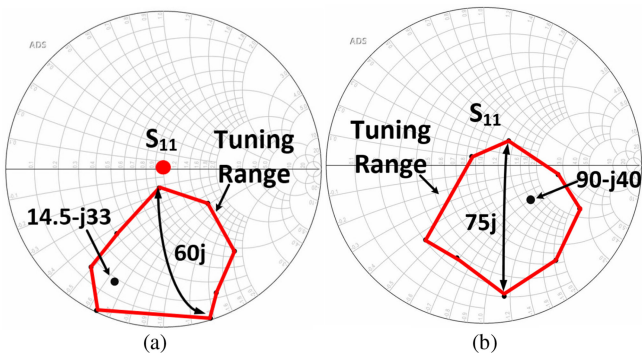
Fig. 16. Measured tuning range of the adaptive matching network at (a) 433 MHz and (b) 915 MHz.

Fig. 17. Measured adaptive matching ability of the auto tuning network in response to a shift in the load impedance: (a) from 50 Ω to (14.5-j33) Ω at 433 MHz, and (b) from 50 Ω to (90-j40) Ω at 915 MHz.

C. Adaptive Matching

Following [27], we have measured the tuning range of the adaptive matching networks and depicted them in Fig. 16. These figures show that if the detuned antenna impedance falls within the red polygon in the Smith chart (including 50 Ω), the adaptive tuning network can help return it back to the matched condition with return loss is below −10 dB. To test the adaptive matching performance, a VNA was used to mimic a 50 Ω antenna. After connecting Tx ASIC to the VNA, the counter in the adaptive matching block was enabled to sweep all of the possible matching conditions, which were recorded to prove the tuning range. To test the matching ability, we selected an exemplar impedance in the matching region in each frequency, here (14.5-j33) Ω and (90-j40) Ω for 433 MHz and 915 MHz, respectively, and monitored the S_{11} measurement results, as shown in Fig. 17. In the ideal case, where the load impedance is 50-Ω, the return loss is below −10 dB. To detune the antenna, the load impedance was changed to (14.5-j33) Ω and (90-j40) Ω for 433 MHz and 915 MHz, respectively, resulting in the return losses greater than −10 dB. The PA output power and efficiency at the two exemplar impedances were also measured. Without adaptive matching, at 433 MHz the output power reduced to −23.48 dBm, showing 3.32 dBm difference. This is corresponding with PA efficiency dropping from 7.53% to 3.72% after impedance change. With adaptive matching, the output power was improved to −20.4 dBm, and the PA efficiency increased to
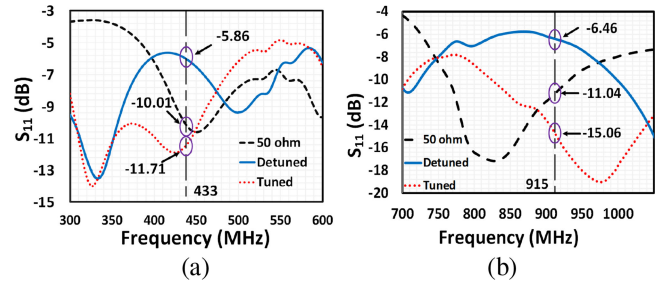
4.51%. As for 915 MHz, 2.2 dBm reduction can be seen at the PA output power without adaptive matching, from −18.77 dBm to −20.97 dBm, dropping the PA efficiency from 8.12% to 5.57%. With the adaptive matching, only 0.18 dBm difference was observed at the output of PA, generating −18.85 dBm output power, corresponding to the PA efficiency of 9.3%. Then the adaptive matching network was allowed to tune the capacitor banks and improve the matching condition. Based on the measurement results, the tuning ranges of the proposed adaptive matching mechanism are up to 60 jΩ and 75 jΩ for 433 MHz and 915 MHz, respectively, as shown in Fig. 16. Table II summarizes and benchmarks the tuning performance of current Tx ASIC prototype.

D. Wireless Communication Link Budget Analysis

To justify if the proposed Tx meets the requirement of our system, a link budget for wireless communication is investigated. The link budget is associated with different losses, such as reflection, absorption, scattering, path loss, and losses due to antenna mismatch [39], [43]. The link margin, L_m, can be calculated using the important parameters listed in Table III. The Tx power is from the measurements in Fig. 15. For reliable communication, [43] suggests maintaining 20 dB link margin. In addition, since the SDR-Rx is an external unit, COTS antennas were considered for 433 MHz [45] and 915 MHz [46]. Fig. 18 shows the distance versus margins for 433 MHz and 915 MHz, which indicates that data can be transmitted from

TABLE III
LINK BUDGET ANALYSIS FOR iTDS WITH DUAL-BAND ANTENNA

Parameters	Variables	Value
Frequency (MHz)	f	433/915
Data Rate (kb/s)	B_r	24
Modulation	OOK	100%
Tx Power (dBm)	P_t	-23.81/-18.77
Tx Ant. Gain (dBi)	G_{TX}	-25.27/-17.13[1]
Path loss (dB)	P_L	Adaptive
Rx Noise Figure (dB)	NF	3.5[2]
Rx Ant. gain (dBi)	G_{RX}	1.2/4[3]
Channel Filter BW (kHz)	BW	540
Signal to Noise ratio (dB)	SNR	12.0[4]
Noise power density (dBm/HZ)	N_0	-203.9

[1]Closed-mouth
[2]From SDR-Rx specifications [44].
[3]From Rx antenna datasheet [45], [46].
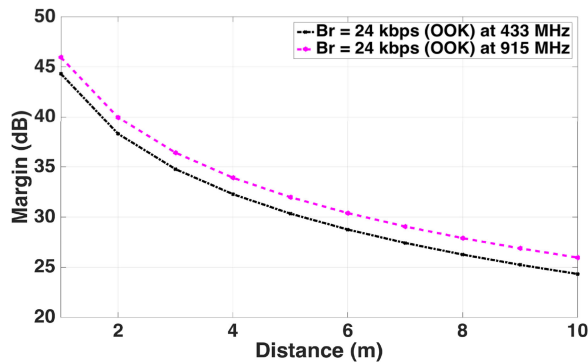[4]Based on the information in [21].

Fig. 18. Distance versus link margin of the dual-band antenna at 433 MHz and 915 MHz at 24 kbps data rate.

distances up to 5 m with 30 dB margins for low gain value at 433 MHz. Similarly, data can be transmitted at distance up to 6 m with 30 dB margin for high gain value at 915 MHz. In iTDS application, the nominal distance between Tx in the user's mouth and SDR-Rx is ~1 m [15], which is well within the link budget according to this analysis.

Implementation of an iTDS prototype in the form of an arch-shaped dental retainer is underway, as shown in Fig. 19. All electronics are housed on two 4-layer FR4 PCBs, connected by a ten-wire flat cable, which are shaped based on the average adult human oral anatomy [17]. The iTDS Tx ASIC and MCU are mounted on one of the two PCBs, with two LSM303D magnetic sensors, one of which is on the backside of the board. To connect the dual-band antenna, a mini U.FL connector is used. The other two magnetic sensors and power management circuitry are mounted on the other PCB. The entire iTDS will be hermetically sealed with a thin layer of Parylene and medical-grade epoxy. Then it will be further protected and given mechanical strength by a self-curing acrylic resin, which is shaped based on the user's dental impression, as commonly done in dentistry. At this stage, stainless steel dental clasps are also embedded in the acrylic to perfectly fit and stabilize the iTDS on the lower teeth.

In a preliminary experiment with the iTDS prototype, the dual-band antenna, coated with PDMS, was connected to the rest
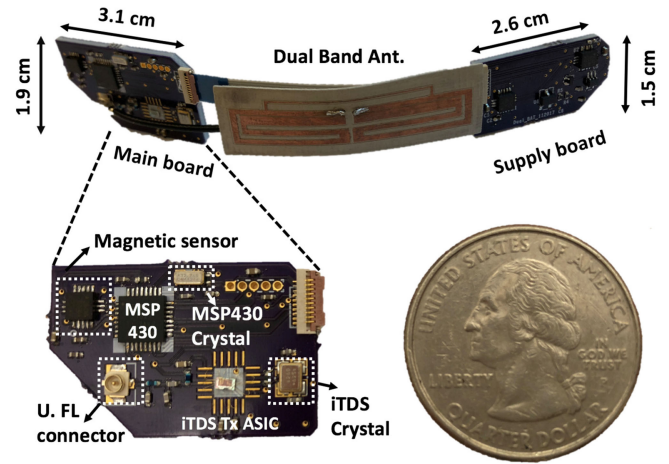

Fig. 19. Implementation of iTDS in the form of arch-shaped prototype with the detailed illustration of the main board.

of the device. A subject placed the sealed iTDS inside the mouth and sat 75 cm away from an Rx antenna, connected to a spectrum analyzer. We asked the subject to open and close the mouth to cause antenna detuning and recorded the received power at 433 MHz and 915 MHz. At 433 MHz, with open and closed mouth, the Rx receives −62.5 dBm and −62.84 dBm signal, respectively. At 915 MHz, the received power is −53.32 dBm and −53.8 dBm for open-and closed-mouth, respectively. The results show that the received power from iTDS is relatively stable under open-and closed-mouth conditions, thanks to the adaptive matching mechanism. In addition, the received power is 30 dB higher than the Rx sensitivity, −106 dBm in this case, from Table III and equations in [47].

V. CONCLUSION

A prototype of adaptive multi-frequency Tx ASIC, operating at 27 MHz, 433 MHz, and 915 MHz is presented with a dual- band antenna for iTDS, a tongue-operated intraoral AT, to establish a robust wireless communication link between the iTDS and an external SDR-Rx. External RF interference can be mitigated by switching the operating frequency from one band to another, which is currently manual, but will be automated in future versions by adding an Rx to this ASIC. Since the Tx antenna is easily detuned in the dynamic mouth environment, increasing the return loss, an adaptive matching network is included by adjustable capacitor banks in the ASIC. They form a feedback loop with an off-chip low power MCU that monitors the output power level, delivered to the Tx antenna, via an on-chip peak detector, to sense the matching condition, and control an on-chip 7-bit up/down counter to adjust the capacitor banks. A small dual-band antenna at 433 MHz and 915 MHz has also been presented, specifically for this application. It has been simulated in HFSS and XFdtd Remcom with a real human head model under open-and closed-mouth conditions. It has also been experimentally characterized and showed enough gain for a robust wireless link, according to the link budget analysis. In the future, the dynamic matching algorithm will be entirely implemented on-chip, and detects interference and switches to a different band in coordination with the SDR-Rx.

REFERENCES

[1] Model System Knowledge Translation Center, "SCI factsheet booklet edition 3 final," 2016. [Online]. Available: http://www.msktc.org/lib/docs/Booklet

[2] R. Barea, L. Boquete, and M. Mazo, "System for assisted mobility using eye movements based on electrooculography," *IEEE Trans. Neural Syst. Rehabil. Eng.*, vol. 10, no. 4, pp. 209–218, Dec. 2002.

[3] J. R. Wolpaw, N. Birbaumer, D. J. McFarland, G. Pfurtscheller, and T. M. Vaughan, "Brain-computer interfaces for communication and control," *Clin. Neurophysiol.*, vol. 113, pp. 767–791, Jun. 2002.

[4] M. R. Williams and R. F. Kirsch, "Evaluation of head orientation and neck muscle EMG signals as command inputs to a human-computer interface for individuals with high tetraplegia," *IEEE Trans. Neural Syst. Rehabil. Eng.*, vol. 16, no. 5, pp. 485–496, Oct. 2008.

[5] Adaptive Switch Labs, Inc. Products. [Online]. Available: http://www.asl-inc.com/products/products.php. Accessed on: Aug. 29, 2018.

[6] NaturalPoint, Inc. SmartNav. [Online]. Available: https://www.naturalpoint.com/smartnav/. Accessed on: Aug. 29, 2018.

[7] Origin Instrument: Sip/Puff Switch. [Online]. Available: http://www.orin.com/access/sip_puff/. Accessed on: Aug. 29, 2018.

[8] L. R. Hochberg *et al.*, "Neuronal ensemble control of prosthetic devices by a human with tetraplegia," *Nature*, vol. 442, no. 7099, pp. 164–171, Jul. 2006.

[9] J. Donoghue, "Bridging the brain to the world: A perspective on neural interface systems," *Neuron*, vol. 60, no. 3, pp. 511–521, Jul. 2008.

[10] C. M. Karat, C. Halverson, D. Horn, and J. Karat, "Patterns of entry and correction in large vocabulary continuous speech recognition systems," in *Proc. SIGCHI Conf. Human Factors Comput. Syst.*, 1999, pp. 568–575.

[11] X. Huo and M. Ghovanloo, "Tongue drive: A wireless tongue-operated means for people with severe disabilities to communicate their intentions," *IEEE Commun. Mag.*, vol. 50, no. 10, pp. 128–135, Oct. 2012.

[12] M. Ghovanloo, M. N. Sahadat, Z. Zhang, F. Kong, and N. Sebkhi, "Tapping into tongue motion to substitute or augment upper limbs," *Proc. SPIE*, vol. 10194, May 2017, Art. no. 1019413.

[13] J. Kim *et al.*, "Tongue enables computer and wheelchair access for the people with high-level disabilities," *Sci. Transl. Med.*, vol. 5, no. 213, Nov. 2013, Art. no. 213ra166.

[14] M. N. Sahadat, A. Alreja, and M. Ghovanloo, "Simultaneous multimodal PC access for people with disabilities by integrating head tracking, speech recognition, and tongue motion," *IEEE Trans. Biomed. Circuits Syst.*, vol. 12, no. 1, pp. 192–201, Feb. 2018.

[15] H. Park *et al.*, "A wireless magnetoresistive sensing system for an intraoral tongue-computer interface," *IEEE Trans. Biomed. Circuits Syst.*, vol. 6, no. 6, pp. 571–585, Dec. 2012.

[16] Nuand, "BladeRF USB 3.0 software defined radio," BladeRF datasheet, 2016.

[17] F. Kong, C. Qi, H. Lee, G. D. Durgin, and M. Ghovanloo, "Antennas for intraoral tongue drive system at 2.4 GHz: Design, characterization, and comparison," *IEEE Trans. Microw. Theory Techn.*, vol. 66, no. 5, pp. 2546–2555, May 2018.

[18] *FCC Online Table of Frequency Allocations*, Federal Communications Commission. [Online]. Available: https://transition.fcc.gov/oet/spectrum/table/fcctable.pdf. Accessed on: Aug. 29, 2018.

[19] International Commission on Non-Ionizing Radiation Protection, "Guidelines for limiting exposure to time-varying electric, magnetic, and electromagnetic fields," *Health Phys.*, vol. 74, pp. 494–5229, 1998.

[20] H. Park and M. Ghovanloo, "An arch-shaped intraoral tongue drive system with built-in tongue-computer interfacing SoC," *Sensors*, vol. 14, no. 11, pp. 21565–21587, Nov. 2014.

[21] H. Park and M. Ghovanloo, "Wireless communication of intraoral devices and its optimal frequency selection," *IEEE Trans. Microw. Theory Techn.*, vol. 62, no. 12, pp. 3205–3215, Dec. 2014.

[22] P. Sjoblom and S. Henrik, "An adaptive impedance tuning CMOS circuit for ISM 2.4-GHz band," *IEEE Trans. Circuits Syst. I, Reg. Papers*, vol. 52, no. 6, pp. 1115–1124, Jun. 2005.

[23] Q. Gu and S. Arthur, "A new method for matching network adaptive control," *IEEE Trans. Microw. Theory Techn.*, vol. 61, no. 1, pp. 587–595, Jan. 2013.

[24] A. Bezooijen, A. Maurice, S. Freek, R. Mahmoudi, and A. H. M. Roemund, "Adaptive impedance-matching techniques for controlling L networks," *IEEE Trans. Circuits Syst. I, Reg. Papers*, vol. 57, no. 2, pp. 495–505, Feb. 2010.

[25] F.C.W. Po *et al.*, "A 2.4 GHz CMOS automatic matching network design for pacemaker applications," in *Proc. Joint IEEE North-East Workshop Circuits Syst. TAISA Conf.*, Jul. 2009, pp. 1–4.

[26] H. Song, B. Bertan, and T. A. James, "A CMOS adaptive antenna-impedance-tuning IC operating in the 850 MHz -to-2 GHz band," in *Proc. IEEE Int. Solid-State Circuits Conf. Dig. Tech. Papers*, Feb. 2009, pp. 384–385.

[27] M. Song *et al.*, "An energy-efficient antenna impedance detection using electrical balance for single-step on-chip tunable matching in wearable/implantable applications," *IEEE Trans. Biomed. Circuits Syst.*, vol. 11, no. 6, pp. 1236–1244, Dec. 2017.

[28] F. Kong, M. Zada, H. Yoo, and M. Ghovanloo, "Triple-band transmitter with a shared dual-band antenna and adaptive matching for an intraoral tongue drive system," in *Proc. IEEE Int. Symp. Circuits Syst.*, May 2018, pp. 1–5, doi: 10.1109/ISCAS.2018.8351709.

[29] *Long Range System Guest Paging Restaurant Pager Wireless Calling Receiver*, Pisector. [Online]. Available: http://www.pisector.com/%20661%20uct&product_id=114. Accessed on: Aug. 29, 2018.

[30] Microsemi, "ZL70101 medical implantable RF transceiver," 2015. [Online]. Available: http://www.microsemi.com/document-portal/zl70101

[31] M. Loy, R. Karingattil, and L. Williams, "ISM-band and short range device regulatory compliance overview," Texas Instruments Appl. Report, May 2005.

[32] B. Lee *et al.*, "An implantable peripheral never recording and stimulation system for experiments on freely moving animal subjects," *Sci. Rep.*, vol. 8, no. 1, pp. 1–12, Apr. 2018.

[33] S. Lee, H. Lee, M. Kiani, and M. Ghovanloo, "An inductively powered scalable 32-channel wireless neural recording system-on-a-chip for neuroscience applications," *IEEE Trans. Biomed. Circuits Syst.*, vol. 4, no. 6, pp. 360–371, Dec. 2010.

[34] H. Schantz and J. Fluhler, "Near-field technology—An emerging RF discipline," in *Proc. Eur. Conf. Antennas Propag.*, Nov. 2006, pp. 6–10.

[35] Y. Yoon, H. Kim, H. Kim, K. Lee, C. Lee, and J. S. Kenny, "A 2.4 GHz CMOS power amplifier with an integrated antenna impedance mismatch correction system," *IEEE J. Solid-State Circuits*, vol. 49, no. 3, pp. 608–620, Mar. 2014.

[36] B. Koo, N. Yoosam, and C. Song, "Integrated bias circuits of RF CMOS cascode power amplifier for linearity enhancement," *IEEE Trans. Microw. Theory Techn.*, vol. 60, no. 2, pp. 340–351, Jan. 2012.

[37] M. Kiani, B. Lee, P. Yeon, and M. Ghovanloo, "A Q-modulation technique for efficient inductive power transmission," *IEEE J. Solid-State Circuits*, vol. 50, no. 12, pp. 2839–2848, Dec. 2015.

[38] Texas Instruments, "Mixed signal microcontroller," MSP430 datasheet, May 2013.

[39] S. A. A. Shah and H. Yoo, "Scalp-implantable antenna system for intracranial pressure monitoring," *IEEE Trans. Antennas Propag.*, vol. 66, no. 4, pp. 2170–2173, Apr. 2018.

[40] F. Kong, S. A. Mirbozorgi, B. Lee, and M. Ghovanloo, "Towards a robust data link for intraoral tongue drive system using triple bands and adaptive matching," in *Proc. IEEE Int. Midwest Symp. Circuits Syst.*, Aug. 2017, pp. 491–494.

[41] A. Bezooijen *et al.*, "A GSM/EDGE/WCDMA adaptive series-LC matching network using RF-MEMS switches," *IEEE J. Solid-State Circuits*, vol. 43, no. 10, pp. 2259–2268, Oct. 2008.

[42] D. Ji, J. Jeon, and J. Kim, "A novel load insensitive RF power amplifier using a load mismatch detection and curing technique," in *Proc. IEEE Radio Freq. Integr. Circuits Symp.*, Jun. 2013, pp. 341–344.

[43] I. Gani and H. Yoo, "Multi-frequency antenna system for skin implant," *IEEE Microw. Wireless Compon. Lett.*, vol. 26, no. 4, pp. 294–296, Apr. 2016.

[44] Lime Microsystem, "Multi-frequency multi-standard transceiver with integrated dual DACs and ADCs," LMS6002D datasheet, Mar. 2012.

[45] Linx Technology, "ANT-433-MHW-xxx-x," ANT-433-MHW-SMA-S datasheet, Mar. 2013.

[46] RF Solutions, "Stubby quad band antenna GSM +4 dB," ANT-GSMSTUB4 datasheet, 2016.

[47] B. Razavi, *RF Microelectronics*. Englewood Cliffs, NJ, USA: Prentice-Hall, 1997.

Authors' photographs and biographies not available at the time of publication.